# High stability of Rh oxide-based thermoresistive catalytic combustion sensors proven by *operando* XAS and XRD

Sabrina Müller,[†] Anna Zimina,[*,‡,†] Ralph Steininger,[¶] Sandra Flessau,[§] Jürgen Osswald,[§] and Jan-Dierk Grunwaldt[†,‡]

[†]*Institute for Chemical Technology and Polymer Chemistry, Karlsruhe Institute of Technology, Germany*

[‡]*Institute of Catalysis Research and Technology, Karlsruhe Institute of Technology, Germany*

[¶]*Institute for Photon Science, Karlsruhe Institute of Technology, Germany*

[§]*Dräger Safety AG & Co. KGaA, Lübeck, Germany*

E-mail: anna.zimina@kit.edu

**Abstract**

Thermoresistive catalytic combustion sensors based on noble metals are very stable stable and highly sensitive devices to monitor potentially explosive atmospheres. We studied and proved the high stability of rhodium oxide-based sensors under working conditions in different $CH_4$/air mixtures (up to 3.5 vol.% methane) with the help of operando X-ray based characterization techniques, DC resistance measurements and IR thermography using a specially designed *in situ* cell. *Operando* X-ray diffraction and X-ray absorption spectroscopy showed that the active Rh species are in oxidized state and their chemical state is preserved during the operation under realistic condition. The resistance correlated with the surface temperature of the pellistor and is related to the combustion of $CH_4$, confirming the catalytic nature of the observed sensing process. Only under harsh operation conditions such as oxygen-free atmosphere or enhanced working current a reduction of the active $Rh_2O_3$ phase was observed. Finally, the effect of the poisoning causing the lowered activity in the catalytic combustion of methane was investigated. Whereas stable rhodium sulfate might form in sulfur poisoned pellistor, silicon dioxide seems to additionally physically block the pores in the alumina ceramics of the pellistor poisoned by hexamethyldisiloxane (HMDS).

## Keywords

Thermoresistive catalytic combustion sensors, gas sensing, pellistor, operando XAS, operando XRD, IR thermography

Wherever flammable gases occur such as in mines, at petrochemical plants or in laboratories, there is an increased risk of explosion. The lower explosion limit (LEL) is the concentration above which the combustion gas/air mixture is ignitable and, once ignited, continues to burn self-sustainingly. The LEL of all known flammable gases lies in the range of 0.5 to 15.0 vol.%, for example, the LEL for methane-air mixtures is 4.4 vol.%[1]. In order to meet occupational health and safety requirements for preventive explosion protection, the gas concentration in potentially hazardous environments must be continuously monitored, by stationary or mobile gas detection devices. As soon as alarm thresholds are exceeded, an alarm is activated, the respective area is evacuated and, if necessary, appropriate countermeasures are taken to prevent the formation of an explosive atmosphere. Nowadays, precise and robust catalytic and optical sensors are used, being able to reliably measure various explosive gases with high sensitivity under demanding and dynamic environmental conditions[2–4]. International standards regulate the performance requirements of gas detectors for flammable gases, i.e., specify maximum permitted deviations of the indication during defined tests for, e.g., long-term stability, poison resistance, linearity, cross sensitivities, air velocity, orientation dependency, time of response, and changes of ambient temperature, pressure or humidity, as well as mechanical robustness against vibration and drop tests[5].

Catalytic combustion sensors have been successfully applied in personal and area monitoring for the past decade due to their high reliability[6–9]. The heat produced by catalytic combustion of the gas at the active element measurably increases the electric resistance of a Pt-wire that acts as the measuring element. The electric resistance is proportional to the concentration of the combustible gas. The advantage of this measurement principle is the direct estimation of the energy content of all flammable gases and vapors, so that catalytic sensors are used as broadband sensors for combustible gases like hydrogen or hydrocarbons (ethane, propene, cyclohexane, methanol, acetone etc.) In contrast, optical sensors, which measure the concentration of a known hydrocarbon in air by analyzing infrared absorption spectra, only indirectly derive the extent of the explosion hazard. Since catalytic gas sensors

are used as broadband sensors for explosive gases, a uniform sensitivity for different gases such as other hydrocarbons is desirable, in contrast to other applications where a high selectivity for catalyst is required. However, one has to consider that the deactivation processes affect the sensitivity of the different compoundss to varying degree.

One of the most common catalytic combustion sensors are so-called pellistors (combination of words "pellet" and "resistor"), which were introduced in 1962[10] and since then continuously developed (cf. refs.[2,4,11,12]). The general structure of such a sensor is depicted in Figures 1 and S1. A thin platinum wire wound into a coil is welded to the gold-plated Kovar feet of a glass feedthrough; the platinum coil is embedded in a porous ceramic bead with a diameter below 1 mm. An electric current through the coil heats the pellet to 450-550 °C. The ceramic bead around the wire contains catalytically active metals like Pt, Pd or Rh and their oxides which enable an efficient and long-term stable catalytic combustion of the gas. For this purpose, the surface temperature needs to be above the activation temperature for the catalytic reaction[2,13,14]. Oxygen for combustion stems from the ambient air, therefore, depending of the type of gas, the minimum required oxygen concentration is 8 to 12 vol.% to ensure excess of oxygen for correct operation. The full combustion of methane is highly exothermic and thus leads to a strong temperature increase of the pellistor[12] according to:

$$\begin{aligned} &CH_4 + 2O_2 \rightarrow CO_2 + 2H_2O \\ &\Delta H_C^{298K} = -890.6 \frac{kJ}{mol} \end{aligned} \tag{1}$$

This increase in temperature causes an increase of the electrical resistance of the Pt metal wire due to the thermoresistive effect.

A conventional catalytic combustion sensor consists of two pellistors: an active detector and a compensator, which are interconnected via a Wheatstone bridge. The compensator is either a catalytically inactive pellistor or an active but significantly diffusion-limited pellistor that does convert no or very little combustible gas. It compensates for environmental effects such as changes of the ambient temperature, humidity and ambient pressure[15]. In presence

of combustible gas, the increase in resistance of the detector leads to an unbalancing of the Wheatstone bridge circuit. A catalytic sensor usually works in the diffusion limit mode: a diffusion barrier like a wire mesh limits the gas exchange rate into the interior of the sensor. A diffusion barrier does not only limit the gas exchange rate into the interior of the sensor but also acts as flame arrestor: if an ignition occurs in the combustion chamber at the surface of the hot pellistors, the flame is cooled down below the ignition temperature when passing the flame arrestor so that the flame cannot penetrate through to the outside, so that the sensor cannot become a source of ignition oneself. Within the measuring range of the sensor, i.e., below the LEL, the combustion gas inside the combustion chamber is converted and the conversion rate of the combustion gas is linear to the temperature increase[16]. Thus the increase in resistance of the Wheatstone bridge is a direct measure for the present concentration of target gas[17].

Stable catalytic combustion of the flammable gases is the key for sensing. However, little is known on the structure of the catalytic component in the pellistor, especially, because hardly any *in situ* or *operando* studies have been reported yet. In general, the catalytic processes exploited in the combustion gas sensing devices are similar to the ones used in emission control applications[18–20]. Despite the operation conditions and the role of the noble metal constituent are slightly different, critical reaction parameters and the susceptibility to certain poisons are similar. Among these parameters, the $O_2$:$CH_4$ feed ratio, the metal loading, the particle size, the nature and the surface (e.g. surface area, porosity) of the support and pre-treatment conditions are the most intensive studied parameters[16,21,22]. In general, noble metal oxide catalysts show higher activity than the corresponding metallic particles and PdO is found to be the most effective metal in the platinum-group-metals (PGMs) for combustion[23–25]. Similar to Pd and Pt catalysts also Rh-based catalysts in their oxidized form are considered to be active[22,23]. In the same way, catalytic combustion sensors under oxygen excess conditions, oxidized Rh in the form of $Rh^{3+}$ is supposed to be the active phase[20]. The $CH_4$ oxidation mechanism on supported noble metal clusters,

which was already in early times[26–28] traced to a Mars-van-Krevelen mechanism (oxidation of the adsorbed educt on lattice oxygen, desorption of the product to the gas phase and the oxidation of the catalyst from the gas oxygen), might be valid for the oxidized particles. A Langmuir-Hinshelwood mechanism (oxidation of two adsorbed educts on the surface and the desorption of the products) has been proposed for metal particles.

Like for PGMs-based catalysts, the deactivation is an important aspect also for pellistors and has been traced back to the sintering or poisoning (a potential deactivation of the catalyst due to blocking the active noble metals or the pores of the ceramic structure). The catalytic activity is usually reduced by the presence of sulfur-containing compounds[29]. The formation of the stable sulfate or/and sulfite species on $PdO/Al_2O_3$ during the $H_2S$ and $SO_2$ exposure was found to be a reason for the deactivation of the catalysts[30]. A similar effect was observed on bi-metallic Pt-Pd particles[31,32]. Rhodium shows usually better resistance to $SO_2$[33] and $H_2S$ poisoning and can be reactivated by treatment in pure $H_2$ or $O_2$ at high temperatures[34,35]. Formation of sulfonate and sulfate during the reforming at 800 °C has been reported for metallic $Rh/Al_2O_3$[36].

Siloxanes are widely used in industrial environments, e.g. as release agents in the plastics industry, for hydrophobing, as building materials and plastics (silicones), in personal care products, in lubricants and oils for machines, and they are parts of landfill and degester gas[37]. Even low concentrations of siloxane (a few ppm) can completely deactivate the catalytic sensor in a very short time. For the same poisoning effect, much higher concentrations of sulphur are required. In addition, high-performance filters for sulfur compounds based on copper and other metal oxides are available. Besides, where sulphur compounds are potentially present, sulphur concentrations are usually monitored for toxicity, while the awareness for the presence of siloxanes is low since it is not relevant for occupational safety. The deactivation of siloxane impurities in methane containing gases has been much less studied[38–40]. During combustion siloxanes can convert into silicon oxide and deposit on the surface, and thus block the pores of the support material or/and the active centers of the metal particles.

The efficient removal of siloxane impurities by filtering the gas stream and the reactivation of the catalysts are still topics of current research.

Although combustible gas sensors are widely used, their structure on the nanoscale, the chemical state of the active phase during operation and the chemical oxidation mechanisms, including the diffusion process to the active sites of the pellistors still lack thorough investigations. Moreover, several questions which are important for the application concerning the aging and the mechanisms of the poisoning of active pellistors resulting in decrease or even complete loss of the gas sensitivity are not clarified yet. The state of the active particles during the reaction is often different from states investigated in ex-situ studies[41], which underlines the importance of monitoring of the chemical state and of the structure of the metallic species under realistic operando conditions of catalysts. The X-ray based spectroscopic methods combined with catalytic characterization methods like mass spectroscopy are widely used nowadays[23,24,42].

In the present study, we shed light on the changes of the chemical state of the active Rh species and the crystalline structure of the pellistors dependent on the treatment history by performing operando Rh $L_3$- and K- X-ray absorption (XAS) and X-ray diffraction (XRD) studies and by combining the results with findings from DC resistance measurements, IR thermography and mass spectroscopy.

# Experimental

**Samples.** The pellistor samples were manufactured by Dräger Safety AG & Co. KGaA (Lübeck, Germany). The ones used in this study consist of a Pt wire of 25 $\mu$m thickness rolled into a coil of 350 $\mu$m diameter surrounded by a porous 15 wt.% Rh-doped ceramic sphere with $\gamma$-$A_2O_3$ as main component. The pellistors were prepared by dropping an aqueous suspension of alumina and a rhodium precursor on the Pt coil, followed by drying applying a heating current through the coil. The subsequent calcination treatment results in a temperature

peak of 800 to 1000 °C for 1 to 2 seconds. Samples were treated differently to simulate the conditioning and poisoning by the $H_2S$ and hexamethyldisiloxane (HMDS) during sensor operation. The pre-treatment conditions of the pellistors studied in this work are listed in Table 1 together with the values of the residual $CH_4$ sensitivity for both poisoned agents. The operation current for this type of Rh-based pellistor in this study was 100 mA. All operando measurements were realized without Wheatstone bridge circuit by directly monitoring the changes in resistance of the active pellistor.

***Operando* cell.** A specially designed *operando* measurement cell depicted in Figure 2 was constructed for the investigation of pellistors with X-ray absorption spectroscopic and X-ray diffraction methods. The cell with a size of 20x40x40 $mm^3$ (32 ml internal volume) contains two large X-ray transparent Kapton windows for the X-ray spectroscopic (both transmission and fluorescence) and scattering experiments. The windows can be exchanged by an infrared transparent foil (Fluoroplastic FEP) for infrared thermographic measurements. In addition, two electrical connectors allow to conduct the DC resistance measurements. The connections for gas inlet and outlet at the cell allowed the precise exposure to varying gas atmospheres controlled by the gas mixing system equipped with mass flow controllers (Bronkhorst, Germany). The subsequent analysis of the product gas mixture was realized with a mass spectrometer (ThermoStar™, Pfeiffer Vacuum, Germany) and, additionally, with a gas chromatograph ($\mu$GC-490, Agilent, Germany) for a quantitative evaluation. The gas inlet and outlet were equipped with twilled Dutch weave (Haver&Boecker OHG, Germany) to ensure the spread of the induced gases and to avoid any turbulence in the cell as pellistors are very sensitive to the smallest disturbances in the gas flow. A total gas flow of 50 mL/min was applied to ensure the steady exchange of the reactive gas mixture in the cell. Applying a current of 5 to 110 mA and monitoring of the change in conductivity of the Pt wire during the exposure of the Rh-based pellistors to different gas atmospheres were realized with the help of a Keithley 2401 device, a combined current source and voltage measure device. Infrared (IR) thermography was performed using a special high performance IR camera (ImageIR

8300, InfraTec, Germany) to evaluate the surface temperature of the pellistors which can be compared to temperatures calculated from the electrical resistance of the Pt wire. The characteristic curves describing the surface temperature dependence on the applied current in air and in reactive gas atmospheres were recorded *a priori* to the *operando* measurements with selected pellistors.

**X-ray absorption spectroscopy measurements.** The structure of rhodium (oxidation state, coordination number) and sulphur (in poisoned catalysts) during sensor operation were examined utilizing X-ray absorption spectroscopy (XAS) at two different beamlines: at the Rh $L_3$ absorption edge (3.004 keV, DCM Si(111)) and at the S K absorption edge (2.472 keV, DCM Si(111)) in fluorescence mode using 7 element Si(Li) solid state detector (SGX Sensortech (MA) Ltd ) at the SULx beamline[43], and at the Rh K absorption edge (23.22 keV, DCM Si(311)) in the transmission mode at the CAT-ACT beamline[44] at the Karlsruhe synchrotron. The size of the beam was set to approx. 100x100 $\mu m^2$ at the SULx beamline and to 750x750 $\mu m^2$ at the CAT-ACT beamline. The ATHENA program of the IFEFFIT package was used for normalization and background subtraction of the X-ray absorption near edge structure (XANES) and extended X-ray absorption fine structure (EXAFS) data[45]. The $k^3$-weighted EXAFS data at the Rh K-edge were Fourier-transformed in the range from 2 to 9 $Å^{-1}$ with the use of a Hanning window with a sill size of 1 $Å^{-1}$. Structural parameters (coordination numbers, bond distance) were extracted by fitting the experimental data from Rh metal and oxide references to the standard crystal structures using the ARTEMIS program. For determining the structural parameters fittings were performed in R-space in the range from 1 to 4 Å, the amplitude reduction factor ($S_0^2$) and the Debye-Waller factor ($\sigma^2$) were set to 0.67 and 0.003, respectively.

**X-ray diffraction measurements.** To determine the crystal structure and to track changes during the operation the pellistors were examined with XRD at 17 keV at the SULx beamline in transmission mode using a CCD detector (Photonic science XDR-VHR 2). One XRD measurement took about 10 min. The experimental $2\Theta$ values were calibrated using

the $LaB_6$ reference and were converted to the inter-atomic spacing values (d, Å) according to the Bragg's law. The particle size L of crystallites was determined from the full width at half maximum of the reflections of the corresponding phase in the XRD data based on the Scherrer equation:

$$L = \frac{K \cdot \lambda}{\Delta 2\Theta \cdot \cos\Theta} \tag{2}$$

with K = 0.89, $\lambda = 0.0723$ nm - the wavelength of X-rays, $\Theta$ - the value of the Bragg angle and $\Delta 2\Theta$ - the full width at half maximum of the selected reflex.

**Operando experiments.** Two different operation conditions were applied during the spectroscopic/scattering experiments. In the first experiment, the conditions resembled standard operation conditions in air: the $CH_4$ concentration was increased from 0.0 to 3.5 vol.% while keeping the oxygen concentration at 21.0 vol.% with $N_2$ as balance. Once the maximal allowed $CH_4$ concentration in air was reached, the applied current was set to 110 mA to study the behavior of the sensor under harsh conditions. In the second experimental series the concentration of oxygen was increased from 0.0 to 21.0 vol.% while keeping the $CH_4$ concentration at 3.0 vol.% and the applied current at 100 mA with $N_2$ as balance gas. With these conditions we aimed at studying the re-oxidation behavior of reduced Rh in dependence on the oxygen concentration. The concentration of $CH_4$ never exceeded the LEL due to safety reasons, nevertheless the experiments should only be conducted by experienced persons and after carefully checking all safety aspects.

# Results

**IR thermography vs. DC resistance measurements.** The IR thermography data were recorded during the exposure of the fresh, conditioned and hexamethyldisiloxane (HMDS) poisoned pellistors, firstly to air with applied current ranging from 5 to 110 mA to obtain the characteristic correlation between the resistance of the pellistor and the surface temperature, and afterwards, the sensors were exposed to the 0.0 to 3.5 vol.% $CH_4$ in air gas mixtures

at a constant current of 100 mA to investigate changes in the resistance and the surface temperature during sensor operation.

Typical IR-thermography images of two fresh pellistors in air at 100 mA working current are shown in Figure S2. From the IR-thermograms one can recognize that the heating of the bead is inhomogeneous over the surface and is strongly influenced by the distribution of the ceramics over the Pt coil at each individual pellistor due to the change in heat transfer through the ceramics. The temperature distribution was measured in the range from 300 to 425 °C across the whole (visible) surface of the bead. The highest temperature is detected in the vicinity of the Pt wire in both samples due to the efficient heat transfer at lower distance. For further analysis the temperature measured by infrared thermography on the surface (denoted as "local surface temperature") has been estimated and then averaged over the surface of the bead (denoted as "surface temperature"). Figure 3 shows the correlation between the surface temperatures derived from IR thermography and the corresponding Pt wire resistance from DC measurements when applying a current from 5 to 100 mA of all pellistors which were studied in pure air. With increase of the current, both the resistance of the Pt wire and the surface temperature of the heated ceramic increased amongst all pellistors. The changes in the temperature in air are nearly linear with a slope of about 50 °C/Ω in the range from 100 to 400 °C (solid red line in Figure 3). The values of the surface temperatures determined by thermography are close to the average temperatures of the heating wire, which can be derived from the DC measurements using the well-known temperature-conductivity relation of bare platinum Figure 3, top axis). There is a difference of about 40 °C at 100 mA applied working current ($\Delta R = 9\ \Omega$) due to the heat loss on the surface of the pellistor to the environment by free convection and radiant heat transfer, e.g. modeled by Kozlov[46].

The IR thermography images of the conditioned pellistor and the distribution of the temperature over the surface during operation with applied 100 mA working current in air, 2.0 vol.% $CH_4$ in air and 5.0 vol.% $CH_4$ in $N_2$ are shown in Figure 4. When the catalytic

reaction occurs at the active pellistor surface in the presence of $CH_4$ and oxygen from the air, the temperature at the surface increases. For instance, in an environment of 2.0 vol.% $CH_4$ in air the consistent increase of the surface temperature by about 180 °C compared to the in-air operation is observed (Figure 4A and 4B). In the absence of oxygen in $CH_4$ in $N_2$ gas mixture no exothermic oxidation reaction takes place and the surface has a temperature of only about 400 °C (Figure 4C). The temperature in $CH_4$ in $N_2$ gas mixture is lower than in pure air because of the more effective cooling of methane with higher heat conductivity compared to air. The temperature and the resistance of all studied pellistors (Figure 3, black symbols and black solid line) changed almost linearly with $CH_4$ concentration reaching a value of about 700 °C ($\Delta R = 15\ \Omega$, the difference to the theoretically calculated temperature of Pt wire is about 85 °C) at 3.5 vol.% $CH_4$ in air except for the HMDS poisoned pellistor (Figure 4, blue symbols). The changes in the temperature in the methane/oxygen containing atmospheres are nearly linear with a slope of about 60 °C/Ω in the temperature range between 400 °C and 700 °C (solid black line in Figure 3), slightly different from the behavior expected from the in-air operation (dashed red line in Figure 3).

Figure 5 shows the changes in the electrical resistance and $CO_2$ concentration in the outlet as a function of the $CH_4$ concentration in the inlet gas mixture. The exothermic methane oxidation at the pellistor surface, proved by the corresponding increase of the $CO_2$ concentration in the outlet of the operation cell, results in an increase of electrical resistance of about 1.8 Ω / vol.% $CH_4$, about 14% of the total volume of injected $CH_4$ is catalytically oxidized (assuming the $CH_4 : CO_2 = 1 : 1$ stoichiometric reaction ratio, see Eq.1). In case of the HMDS poisoned pellistors, the temperature and the resistance value stayed practically constant (average surface temperature at about 440 °C, $\Delta R = 0.5\ \Omega$ independent of the presence of $CH_4$ in the atmosphere). A negligible amount of $CO_2$ is formed (about 1% of the total volume of injected $CH_4$), i.e., the catalyst is effectively poisoned by the HMDS leading to essentially no electrical response.

**Operando XRD and XAS: chemical state of Rh vs $CH_4$ concentration.** The

XAS and XRD data were recorded during the exposure of fresh and conditioned pellistors to the 0.0 to 3.0 vol.% $CH_4$ in air with an applied current of 100 mA to investigate changes of the chemical state and in the crystalline structure of the Rh particles during operation. Harsh conditions (110 mA working current and oxygen-free atmosphere) were applied to the fresh sensor to test the stability of the sensors in terms of the ability to regenerate.

Figure 6 shows the Rh $L_3$- and K-XAS data of fresh and conditioned pellistors at different operation conditions together with the reference data of metallic Rh and $Rh_2O_3$. The energy position and the shape of the XAS spectra at both absorption edges measured on fresh and conditioned pellistors in air with the applied current are close to the ones for the $Rh_2O_3$ reference, hinting to mainly $Rh^{3+}$ as chemical state of the rhodium at this stage. However, small differences are seen in the shape of the XANES spectra of the fresh and conditioned pellistors compared to the reference materials and between them hinting to the presence of non-stoichiometric oxide species in the initial state and/or to the different $Rh^0/Rh^{3+}$ ratios in the sensors due to different pre-treatment. At the Rh K absorption edge the intensity of the white line at 23.231 keV is about 10% lower and the shape of the post-edge feature is altered (feature at 23.242 keV is slightly shifted to higher energies) in case of the conditioned pellistor compared to the fresh one (Figures 6A, curves h). To evaluate the amount of Rh and $Rh_2O_3$ in the ceramic bead all the XAS data at both Rh $L_3$ and K absorption edges were deconvoluted to the single components corresponding to the $Rh^0$ and $Rh^{3+}$ contributions using the linear combination analysis (LCA) package of Athena[45]. The results of this procedure are displayed in Figure S3. The samples at the 100 mA working current in air showed the presence of $Rh^{3+}$ species of about 80±2% (average between K and $L_3$ XAS) in fresh and 82±2% (50±2% from XAS $L_3$) in conditioned pellistors. This ratio and the spectral shape of the Rh XAS at both edges stay practically unchanged during the operation at 100 mA with the increase of the $CH_4$ concentration.

During the exposure to the $CH_4$/air mixture with 100 mA and with 10% enhanced working current no significant changes in the shape of the XAS spectra were observed (Figure 6,

curve d). This confirms that the $Rh^{3+}$ chemical state is preserved during normal and harsh operation conditions and shows the high stability of the catalytic component. A significant reduction of $Rh^{3+}$ to Rh metal only occurred in oxygen-free atmosphere (Figure 6, curves e and f). In this case Rh is found in nearly 100% reduced state. The intensity ratio of the characteristic features in the spectrum obtained at 5.0 vol.% $CH_4$ in $N_2$ is slightly different from the metallic rhodium in both fresh and conditioned pellistors which may indicate that the reduction of the Rh in oxygen-free atmosphere is not completed (about 5% oxidized species remained according to the LCA analysis of $L_3$-XAS data, Figure 8) and/or modified crystalline structure of the nanometer-sized Rh particles compared to the bcc-Rh.

The Fourier transformed $k^3$-weighted EXAFS spectra at the Rh K-edge data of fresh and conditioned pellistors in air are shown in Figure 7 together with the data of the reference materials. The Rh-O peak of $Rh_2O_3$ at 1.8 Å are clearly seen in the data of both the fresh and the conditioned pellistors in all oxygen containing atmospheres, the appearance of the Rh-Rh backscattering peak at 2.2 Å of metallic Rh is first seen in oxygen-free operation conditions (Figure 7, curve e). The lack of the long-range order in catalytically active Rh-particles is observed in oxidized Rh pellistors, in reduced pellistors second and even third coordination shells are found (Figure 7, curve e, peaks at 3.6 and 5.0 Å). Results of the fitting of the EXAFS data to the reference structures (Table S1) confirmed the existence of Rh-O bonds in the oxidized species with the bond length close to the values of the bulk material and slightly reduced coordination numbers in Rh-Rh coordination shells.

The XRD measurements (Figure 8) revealed that the support material is present in the form of $\alpha$-$Al_2O_3$ (well distinguished diffraction peak of $\alpha$-$Al_2O_3$ $(10\overline{2})$ at 3.47 Å and $(21\overline{3})$ at 2.2 Å), in contrast to the initially expected $\gamma$-$Al_2O_3$. The presence of the $\alpha$-form might be explained by the high temperature treatment (approx. 800-1000 °C) that is reached during the calcination reaction, causing the phase transition of the alumina. The narrow Pt reflection at d = 2.3 Å in the diffractogram of the conditioned pellistor originates from the Pt wire (fcc-Pt (111) diffraction peak) inside the pellistor bead being hit by the beam. The

initial state of Rh in the fresh and conditioned sensors at 100 mA in air is found to be $Rh^{3+}$ in the structure close to the orthorhombic crystalline structure of $Rh_2O_3$ (broad features close to the position of (114) and (020) diffraction peaks of oxide at around 2.6Å). However, a non-negligible and broad diffraction peak at the metallic Rh (111) reflection at 2.2 Å is also visible in the diffractogram of the conditioned pellistor in air at 100 mA operation current (Figure 8, curve b) corroborating the earlier postulated finding of the possible presence of reduced Rh in conditioned pellistor (Rh $L_3$ XAS). This peak diminished readily in air/$CH_4$ atmospheres during operation and could no longer be observed in 1.0 vol.% $CH_4$ in air at 100 mA (Figure 8, curve c). During normal sensor operation in air containing different $CH_4$ concentrations no changes in the crystal structure of the oxide was observed, neither in fresh nor in conditioned pellistors. No significant reduction of the $Rh_2O_3$ to metallic Rh was observed until the increase of the applied current to 110 mA and the removal of the oxygen from the reactive gas mixture (Figure 8, curve h: reflections at the positions of the fcc crystal structure of Rh (111) and (200) at 2.2 Å and 1.8 Å).

Based on the Scherrer equation (Eq.2) using the Rh(111) reflection the crystallite size of the formed metallic Rh particles in the reduced pellistors was estimated to 64±2 Å. The particle size of $Rh_2O_3$ species in the initial state could not be determined accurately due to the strong overlapping of the several broad diffraction peaks. Nevertheless, the extreme broadening and low intensity of the oxide related XRD reflections (together with the lack of the long-range order, seen in Rh K EXAFS) hints to the presence of small oxidized species in the case of both fresh and conditioned pellistors, possibly in form of dispersed layers or shells on metallic cores.

**Operando XAS and XRD: Chemical state vs. oxygen concentration.** The XAS (Figure 9) and XRD (Figure 10) data was recorded in a next step during the exposure of the fresh pellistor, first to reducing gas mixture (3.0 vol.% $CH_4$ in $N_2$, 100 mA) and then to 3.0 vol.%$CH_4$ in $N_2$ gas mixture with increasing concentration of oxygen at a constant current of 100 mA to investigate the concentration of the oxygen required for the re-oxidation of the

Rh particles and to explore the sensing behavior during such operation conditions. The fresh pellistor which contained about 80% $Rh^{3+}$ species was reduced in oxygen free atmosphere to nearly 100% metallic state. The LCA analysis of the chemical state of the active Rh species depending on the oxygen concentration in the reactive atmosphere showed that the metallic Rh particles start to oxidize in the presence of at least 6.0 vol.% of oxygen and rapidly approached to the values of the initial states at 10.0 vol.% of oxygen. Moreover, the increase of the intensity of the reflections of metallic Rh (marked with blue lines in Figure 10) and decrease of the diffraction peaks of the Rh oxide (marked with red lines in Figure 10) the exposure to 2.0 vol.% of oxygen indicates further reduction of Rh and possible sintering of the metallic particles under oxygen lean conditions. The analysis of the EXAFS data at the Rh K-edge (Table S1) confirmed the formation of the Rh-Rh bonds close to bcc-Rh in reduced pellistors and reoxidation of Rh in the atmospheres with the oxygen concentration above 6.0 vol.%. The XRD and XAS data revealed that the Rh preserved its reduced state and the fcc crystalline structure in 3.0 vol.% $CH_4$ atmospheres containing up to 6.0 vol.% $O_2$ without significant formation of $Rh_2O_3$-like structures. Under these conditions the operation of the pellistor was still possible as the $CH_4$ combustion still took place causing the changes in the resistance of the pellistor. However, the behavior was strongly changed, probably strongly influenced by the metallic character of the active Rh particles which changed the thermal conductivity of the ceramic bead and its catalytic efficiency, as the resistance first increased with the increase of the $O_2$ concentration to $\Delta R = 14\ \Omega$ (the measured surface temperature of about 600°C) in 6.0 vol.% $O_2$ and then decreased again to $\Delta R = 12\ \Omega$ (the measured surface temperature of about 700 °C). The overall description of the pellistor response with the oxygen concentration governed by the chemical state of the majority of Rh particles is presented in Figure 11.

***Ex situ* XRD and XAS: effect of $H_2S$ and HMDS poisoning.** Two differently poisoned samples were investigated. Both HMDS and $H_2S$ poisoned pellistors were measured at Rh $L_3$ absorption edge (Figure 6A) and with XRD (Figure 8) to examine the structural

changes due to the different poisoning. Additionally, the HMDS poisoned pellistor was measured at Rh K absorption edge (Figure 6B) to examine the location of the Si species. Non-negligible differences in the shape of the XANES spectrum of both poisoned pellistors compared to the conditioned pellistors are seen which could hint to the modification of the Rh-O bond by a non-metallic compound. At the Rh K absorption edge the intensity of the white line at 23.231 keV is about 20% lower and the shape of the post-edge feature is altered (the intensity of the feature at 23.242 keV is slightly reduced) in case of the HMDS poisoned pellistor compared to the conditioned one (Figures 6B, curves g). The intensity of the white line at the Rh $L_3$-edge is significantly decreased and additionally shifted to lower energies in case of both poisoned pellistors (Figures 6A, curves g and g*).

The LCA of the *ex situ* Rh K and $L_3$ XAS data of the HMDS poisoned pellistor corroborate the higher metal content compared to the conditioned pellistor with the $Rh^{3+}/Rh^0$ ratio of 67 : 33 (the ratio in conditioned pellistor is 82 : 12). The Fourier-transformed EXAFS Rh K data recorded on HMDS poisoned pellistor is shown in Figure 7. The intensity of the Rh-O peak at 1.8 Å is reduced and an additional peak at 2.2 Å appeared compared to the conditioned pellistor, confirming the changes in the chemical bond of rhodium due to the Si presence. The position of this peak indicates the presence of the non-metallic element in the vicinity of the oxygen ions different from the rhodium (peak corresponding to the Rh ion in the second shell in the $Rh_2O_3$ is expected at the 2.8 Å, peak of the Rh in the first shell in the metallic rhodium - at 2.7 Å, see FT EXAFS data of reference material in Figure 7). In the XRD pattern of the HMDS poisoned pellistor only weak reflections which may correspond to the Rh (111) reflection can be recognized (Figure 8).

The LCA of the *ex situ* XAS Rh $L_3$ data of the $H_2S$ poisoned pellistor revealed the lower metal content compared to the conditioned pellistor with the $Rh^{3+}$ / $Rh^0$ ratio of 96 : 4. In the XRD pattern of the $H_2S$ poisoned pellistor no reflections corresponding to the Rh(111) reflection can be recognized (Figure 8), confirming the oxidation effect of $H_2S$. The XAS S K data recorded using this pellistor (not shown here ) indicate the presence of $S^{6+}$ and $S^{4+}$

species, hinting to the formation of sulfates and sulfites in poisoned pellistor, different from the $Al_2(SO_4)_3$[34,42,47].

## Discussions

The active sites in the pellistors under normal operation conditions (100 mA working current and excess of oxygen) in this study are oxidized Rh particles that catalyze the combustion of methane. Similarly as reported for Pd-based methane oxidation catalysts, methane is expected to adsorb on the Rh oxide entities whereby lattice oxygen can oxidize methane in Mars-van-Krevelen mechanism as discussed above. The resulting vacancies are quickly filled up by oxygen from the gas phase. The present study shows that the Rh-oxide particles are very stable under reaction conditions, as they neither reduce nor form large particles in agreement with XAS/XRD. While a conditioning of the pellistor in form of a long exposure to a mixture of the reducing gases and air might lead to the partial reduction of $Rh^{3+}$, such reduced species are found to be quickly re-oxidized under normal operation conditions.

In air with the $CH_4$ concentration between 1.0 and 3.0 vol.% (corresponding to 10 and 80% of LEL in Europe) and with relatively high Rh-loading, the electrical response of the pellistor is thus stable and proportional to the $CH_4$ concentration. Deficit of oxygen in the working atmosphere causes a non-linear response of the sensor governed by the metallic character of the active Rh species. The electrical response is related to the total resistance of the pellistor: it reflects changes of the temperature of the ceramic bead and depends on the thermal conductivity of the $Rh_xO_y/Al_2O_3$ material. For the case of metallic Rh, the surface temperature and the electrical resistance is linear dependent on the oxygen concentration hinting to the direct reaction of the educts on the surface of Rh with the heat formation corresponding to the concentration of the oxygen.

After normal operation (at temperatures about 500-600 °C) for several hours and controlled exposed to the $H_2S$ gas the enhancement of Rh-O bond strength in the presence of

sulfur might indicate the formation of the rhodium sulfate causing the chemical blocking of the active oxygen leading to irreversible poisoning of the pellistors. The adsorption of the $H_2S$ on O-Rh sites with following rhodium sulfite and sulfate formation due to the reaction with oxygen from the reactive gas mixture similar to the mechanism proposed for the $PdO/Al_2O_3$[30] and $Rh/Al_2O_3$[33]but without the formation of the aluminum sulfate might also be applicable in this case of poisoning.

The pellistor poisoned in HMDS is very much deactivated. The reduction of the $CH_4$ sensitivity is reflected by a drastic reduction of the response signal, the $CO_2$ formation and surface temperature. A weakening of Rh-O bonds in the presence of $SiO_2$ might indicate a direct blocking of the active sites. Another possible explanation of the deactivation might be the adsorption of the $SiO_2$ in the pores of alumina and then in a physical way blocking of the active rhodium species.

# Conclusions

A novel *in situ* cell has been designed to study catalytic gas sensors (pellistors) under operating conditions. The *in situ* cell allows to apply both spectroscopic and scattering methods and allowed to combine for the first time operando X-ray based methods (XANES, EXAFS, XRD) and IR thermography. Both the structure and the variations in the surface temperature of an active element of miniature catalytic combustion sensors was monitored under working conditions while determining the sensor performance using the resistivity. Hence, changes in resistivity were successfully compared to the surface temperature of the pellistor measured by IR thermography and to the crystalline structure and the chemical state of the active Rh species. The resistance correlated with the surface temperature of the pellistor and related to the combustion of $CH_4$, confirming the catalytic nature of the observed sensing process.

XAS and XRD measurements of the freshly prepared and conditioned pellistors revealed

that the active Rh species during sensor operation under normal operation conditions are oxidized structurally close to $Rh_2O_3$ but more amorphous. The investigated samples showed high stability of the chemical structure and reliable electrical response in gas atmospheres below the LEL of $CH_4$ in air. The active oxidized chemical state of Rh and the particle size did not change until the oxygen concentration was below the stoichiometric mixture needed for the combustion reaction. Only under harsh conditions (oxygen concentration below 6.0 vol.% and enhanced electrical current) rhodium was reduced. At such conditions the active $Rh^0$ species were observed and the sensing signal showed non-linear behavior as response to the changes in $CH_4$ concentration.

Poisoned sensors demonstrated lowered activity in the catalytic combustion of methane, hinting to the blocking of active species due to modification of the Rh-O bond by $SiO_2$ or S; whereas stable rhodium sulfate might form in sulfur poisoned pellistors, $SiO_2$ additionally seems to physically block the pores in alumina in HMDS poisoned pellistors.

These results of the first systematic and *operando* characterization study of the influence of the pretreatment condition of the sensor on the sensor performance give further insights into the structure-function relationships of Rh nanoparticles and will help to optimize the performance of the miniature catalytic combustion sensors in future.

## Acknowledgement

The Team Catalytic Gas Sensors of the company Dräger Safety AG & Company KGaA (Germany) is acknowledged for the opportunity to investigate catalytic combustion sensors in collaboration and providing the sample materials. The authors thank the Institute for Beam Physics and Technology (IBPT/KIT) for the operation of the storage ring in the Karlsruhe Reasearch Accelerator (KARA). We acknowledge Dr. T. Prüßmann, the beamline scientist at CAT-ACT beamlines at KIT synchrotron facility, for the support during the measurement periods.

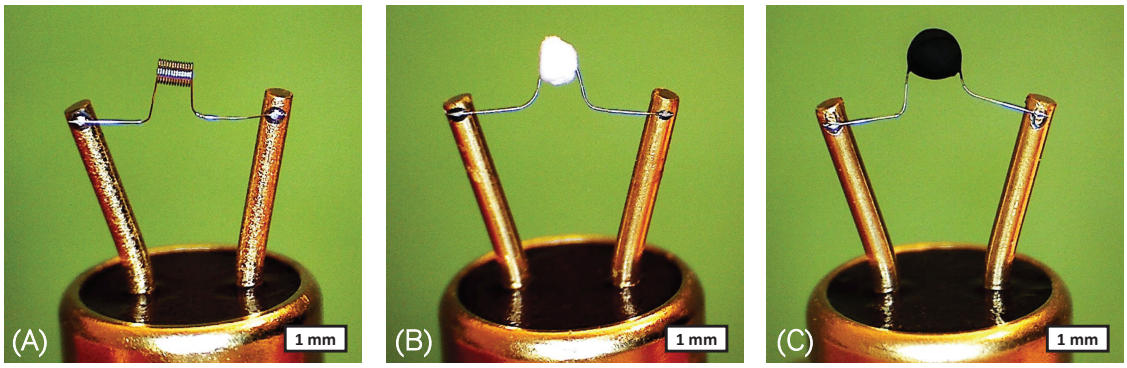


Figure 1: Photographs of (**A**) a glass feedthrough with a platinum coil welded to its feet, (**B**) a catalytically inactive, compensating pellistor, and (**C**) a catalytically active, detecting pellistor.

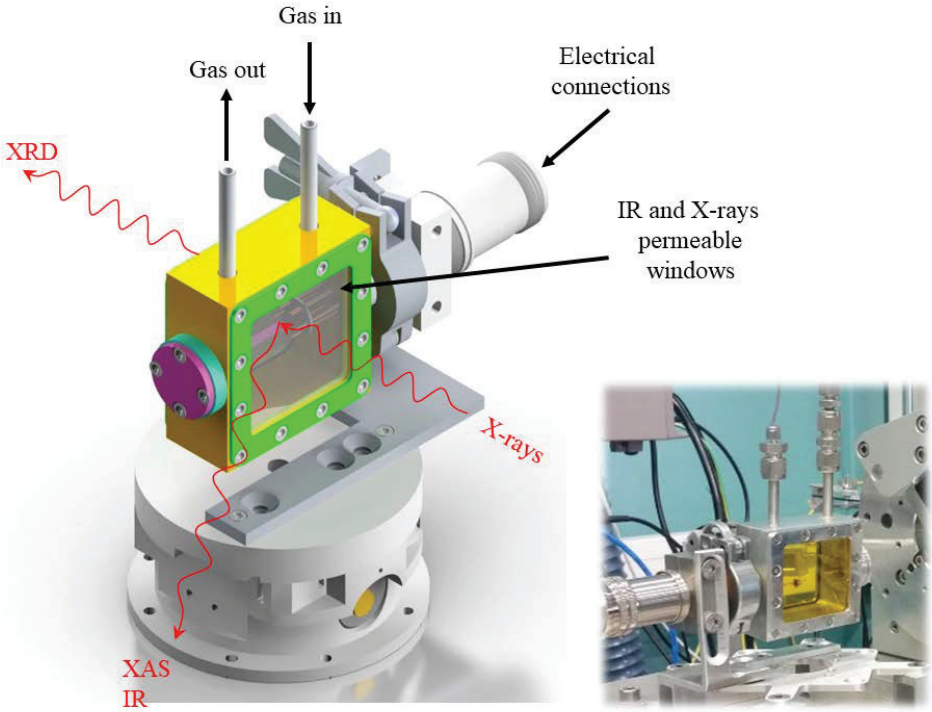


Figure 2: *Operando* cell suitable for XRD, XAS and IR measurements with simultaneous read-out of electrical properties. The cell is equipped with IR and X-ray permeable windows, gas inlet and outlet with a twilled dutch weave for an optimal diffusion of the incoming gas.

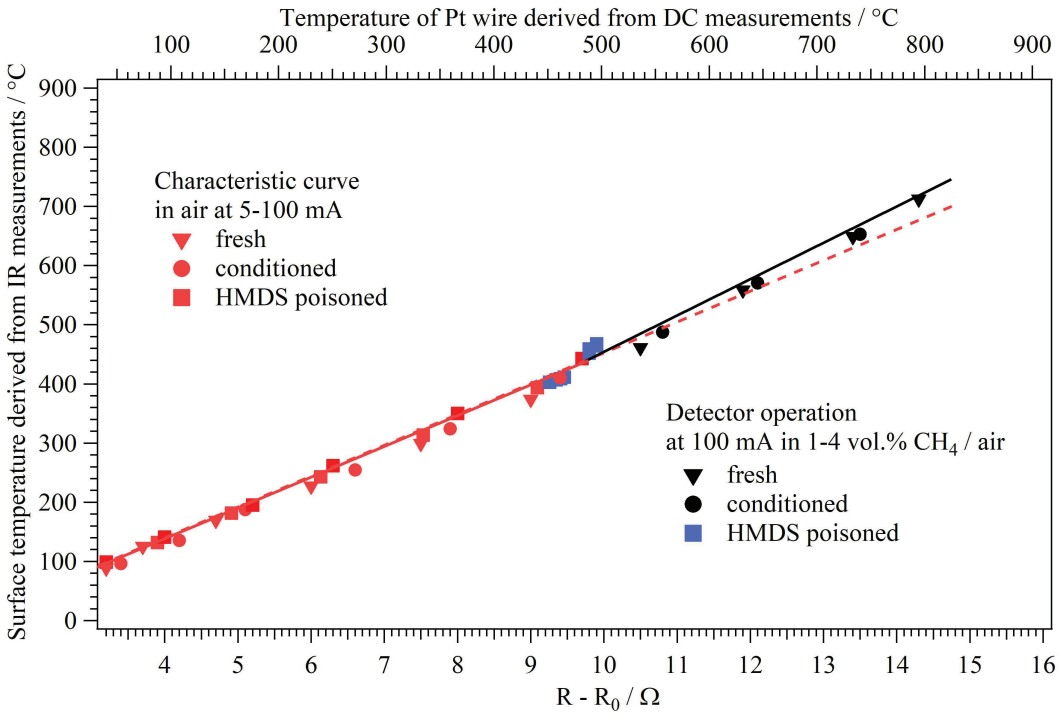


Figure 3: Average surface temperature - resistance correlation in air during heating of a fresh (triangle), a conditioned (circles), and an HMDS poisoned (squares) pellistor by applying 5 to 100 mA current (red symbols), and under $CH_4$ containing atmospheres at a working current of 100 mA (black and blue symbols). Lines as guides for the eye.

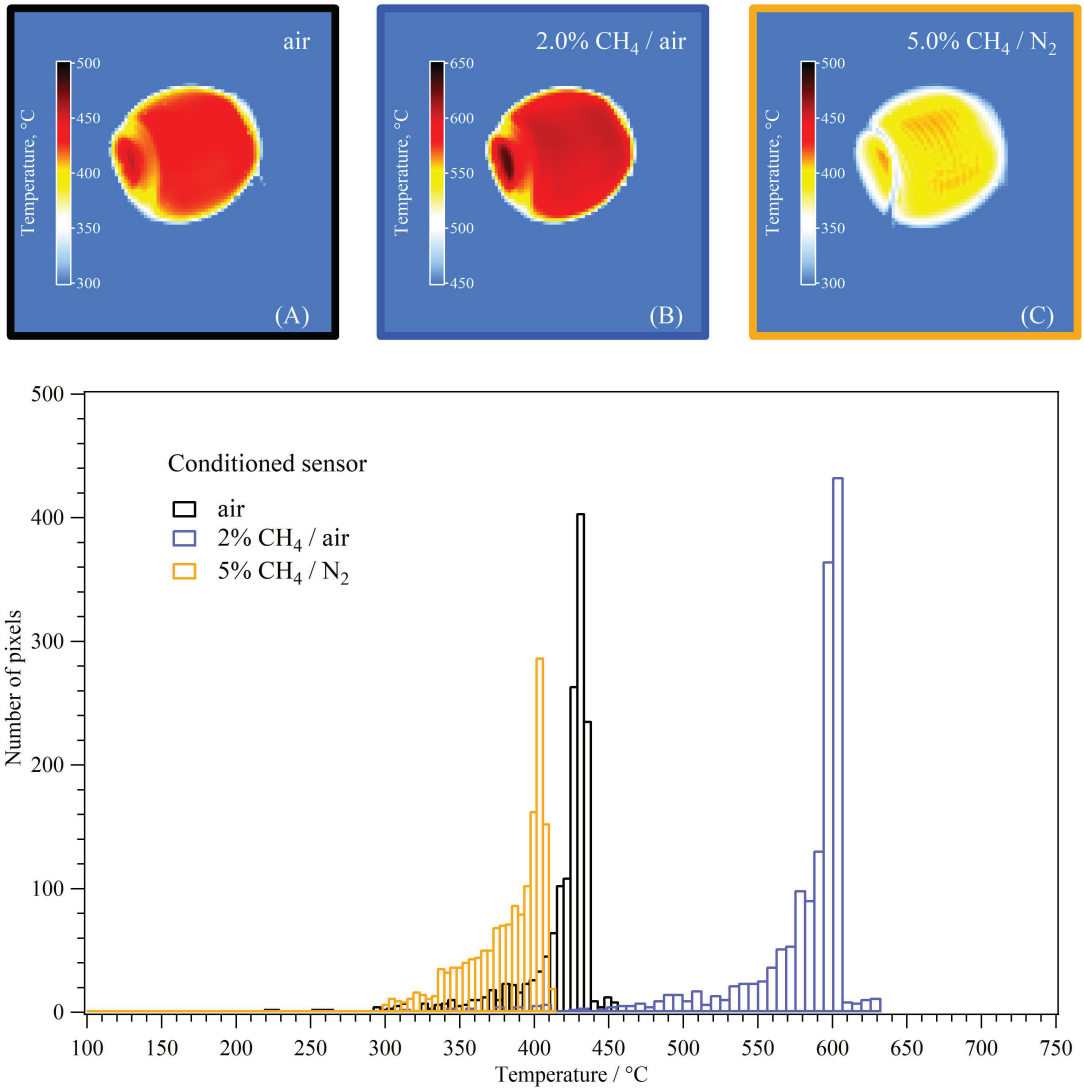


Figure 4: Thermograms of a conditioned pellistor at 100 mA operation current in $CH_4$ containing atmospheres (air (**A**), in 2.0 vol.%$CH_4$ in /air (**B**) and in 5.0 vol.%$CH_4$ in $N_2$ (**C**)) and distribution of the local surface temperature over the pellistor at different conditions.

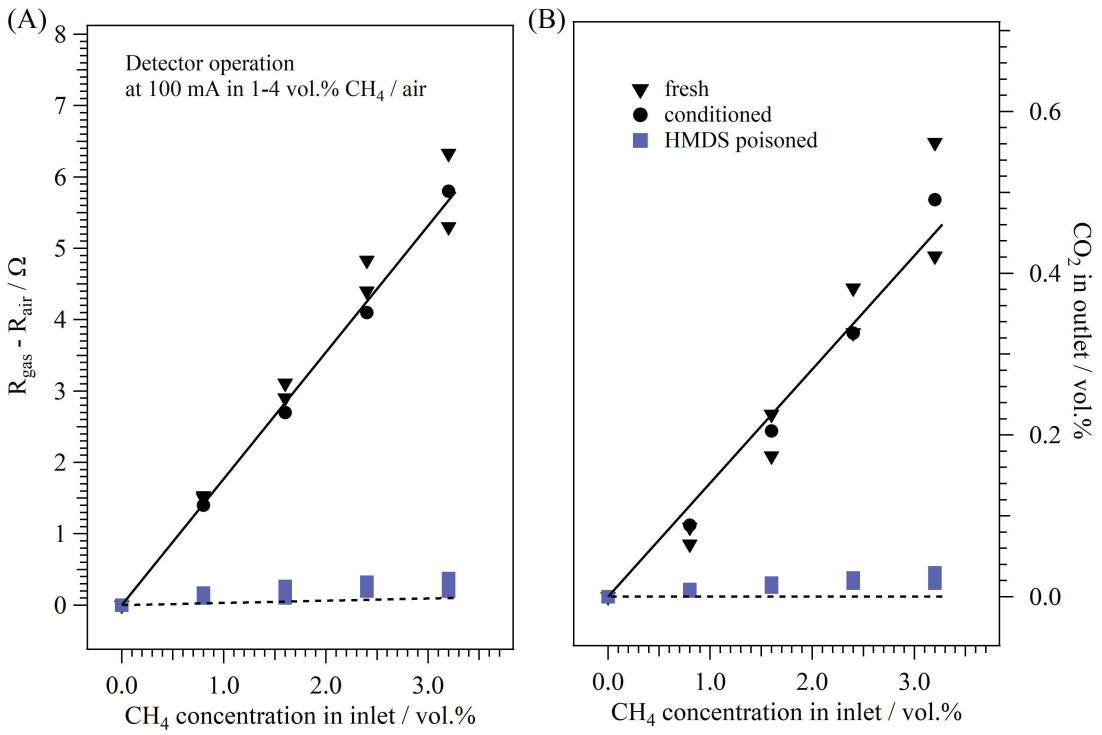


Figure 5: Correlation between (**A**) the electrical response, (**B**) concentration of the $CO_2$ (product of the partial methane oxidation) and the $CH_4$ concentration in the air atmosphere of the fresh (triangle), conditioned (circle), and HMDS poisoned (square) pellistors at 100 mA working current. The $CO_2$ and $CH_4$ concentrations were measured with $\mu$GC.

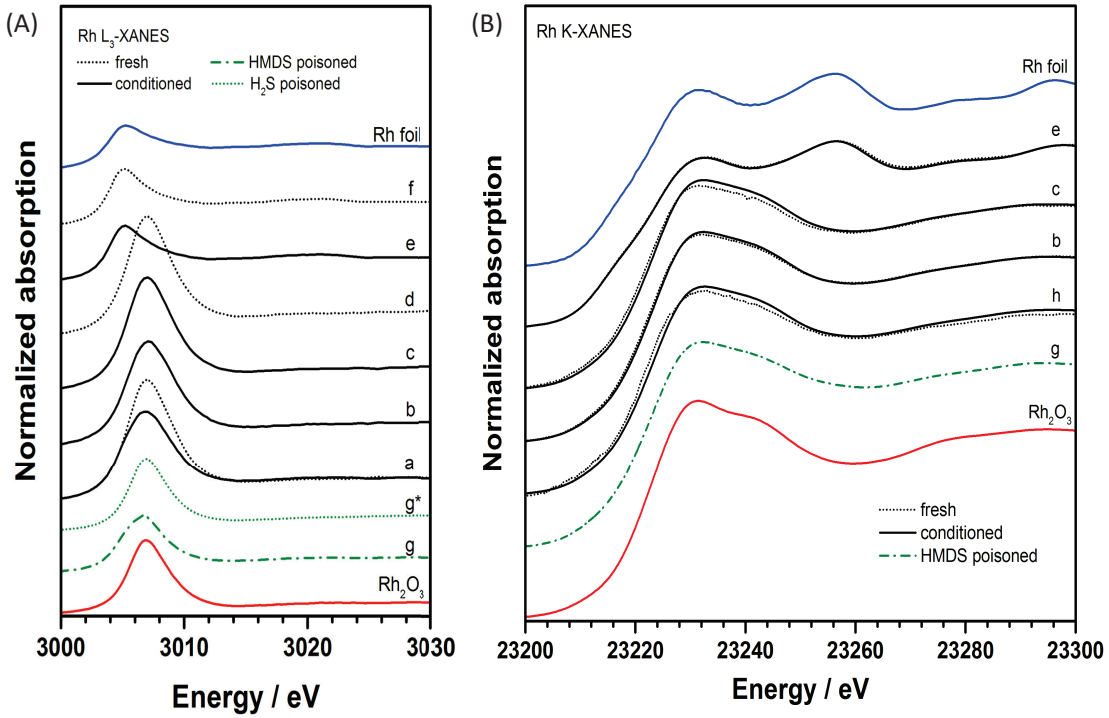


Figure 6: *Operando* XAS at the Rh $L_3$- (**A**) and K-edges (**B**) of a fresh and a conditioned pellistor in different $CH_4$/air atmospheres at different working currents: (a) air/100mA, (b) 1.0% $CH_4$/air/100mA, (c) 3.5% $CH_4$/air/100mA, (d) 3.5% $CH_4$/air/110mA, (e) 5.0% $CH_4/N_2$/100mA, (f) 5.0% $CH_4/N_2$/110mA, (h) air/0mA. The poisoned pellistors were measured ex-situ (g, g*). Rh foil and $Rh_2O_3$ powder were used as references.

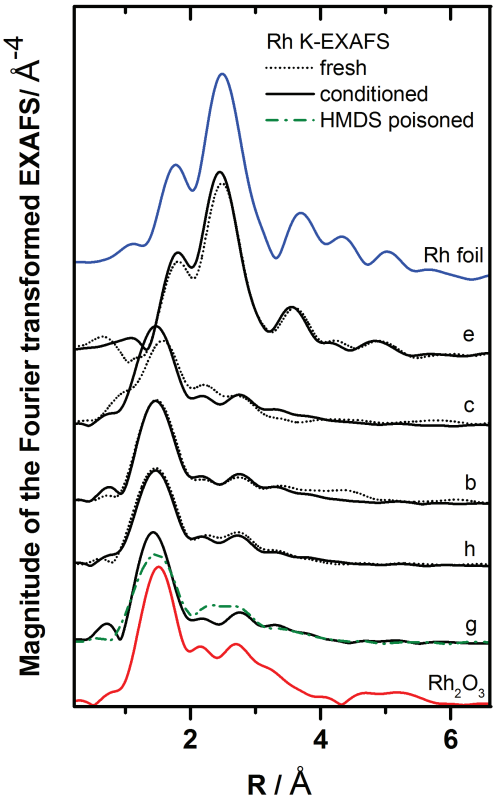


Figure 7: Fourier transforms of $k^3$-weighted EXAFS data of fresh, conditioned and HMDS poisoned pellistors during *operando* XAS in different $N_2$ or air/$CH_4$ atmospheres and different working current at the Rh K-edge: (g) $N_2$/0mA, (h) air/0mA, (b) 1.0% $CH_4$/air/100mA, (c) 3.5%$CH_4$/air/100mA, (e) 5.0% $CH_4$/$N_2$/100mA. The HMDS poisoned pellistor is measured ex-situ. Rh foil and $Rh_2O_3$ powder were used as references.

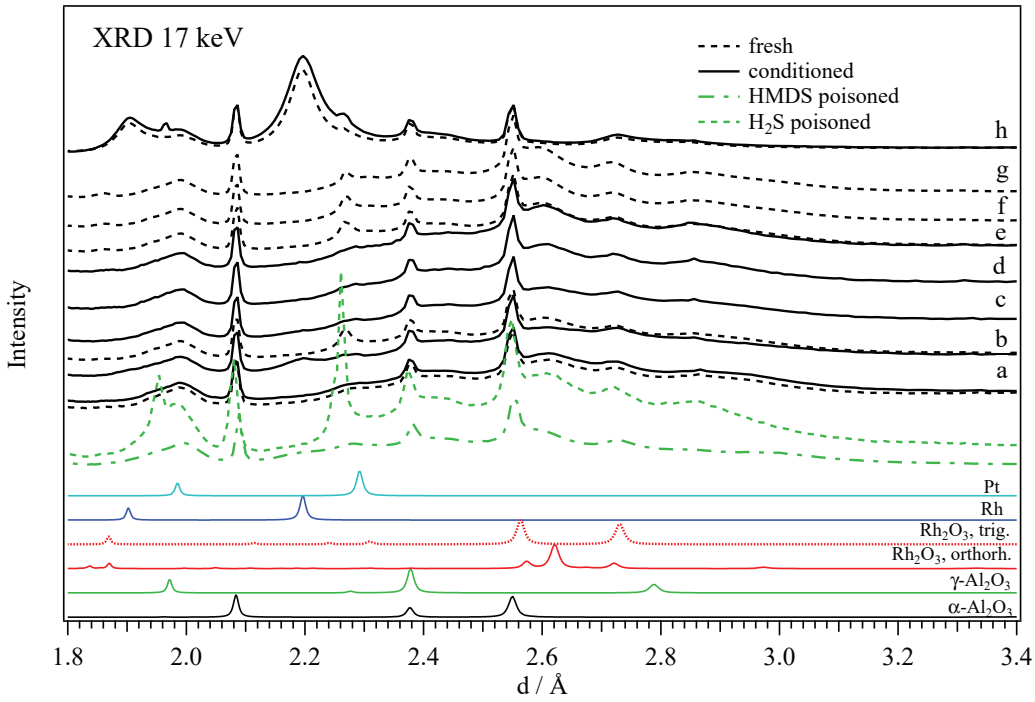


Figure 8: *Operando* XRD patterns of fresh and conditioned pellistors in different $CH_4$/air atmospheres at different working current: (a) air/0mA, (b) air/100mA, (c) 1.0% $CH_4$/air/100mA, (d) 2.0% $CH_4$/air/100mA, (e) $\alpha$-$Al_2O_3$ $(10\overline{2})$ reflection at 3.48 Å. The XRD of HMDS and $H_2S$ poisoned pellistors were measured *ex situ*.

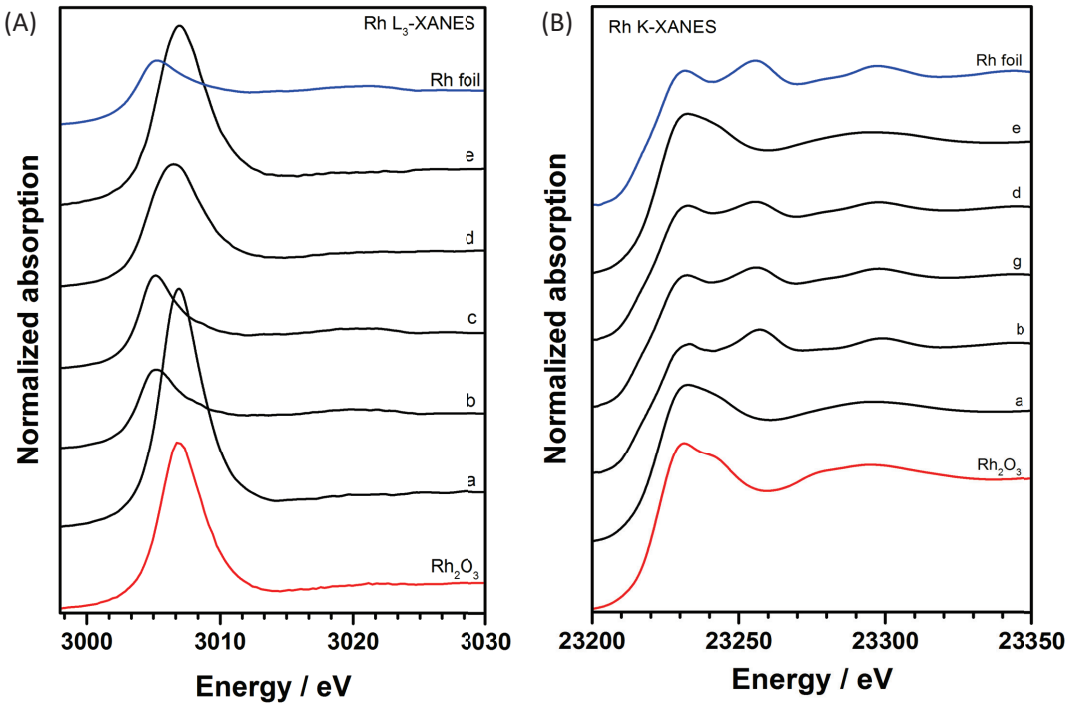


Figure 9: *Operando* XAS at the Rh $L_3$-edge (**A**) and K-edge (**B**) of a fresh pellistor at 100 mA working current in air (21.0 vol.% $O_2$) (a) and in 3.0 vol.% $CH_4$ with different $O_2$ content: (b) 0.0 vol.%, (c) 2.0 vol.%, (g) 3.0 vol.%, (d) 6.0 vol.%, (e) 10.0 vol.%. Rh foil and $Rh_2O_3$ powder were used as references.

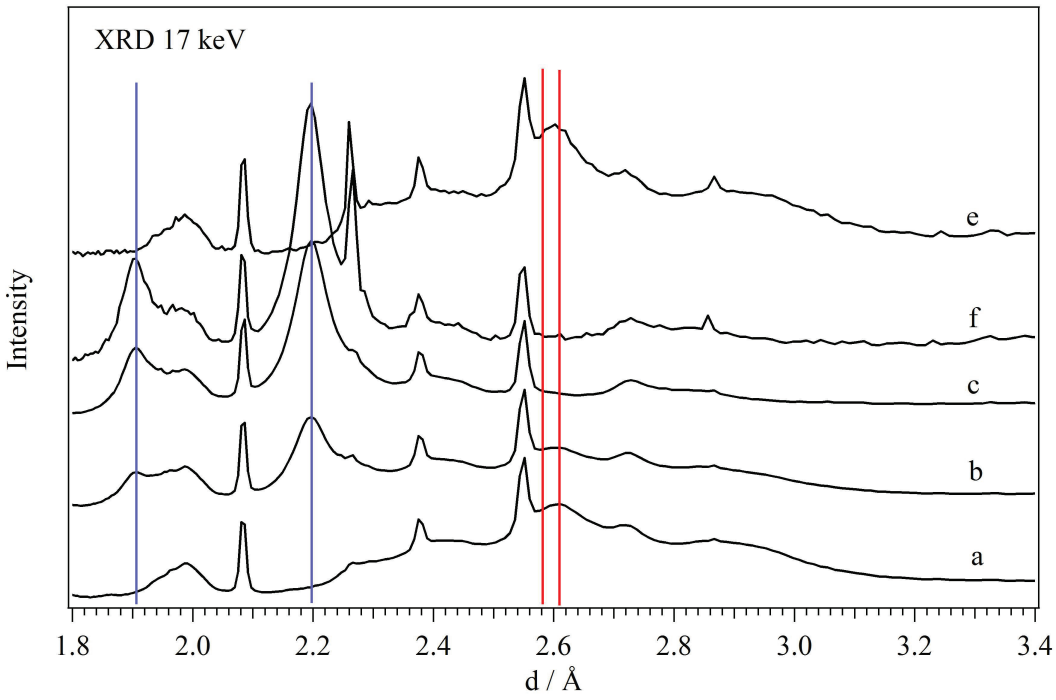


Figure 10: *Operando* XRD of a fresh pellistor measured at 100 mA working current in air (21.0 vol.% $O_2$) (a) and in 3.0 vol.% $CH_4$ with different $O_2$ content (using $N_2$ as balance): (b) 0.0 vol.% (c) 2.0 vol.%, (f) 5.0 vol.%, (e) 10.0 vol.% . The positions of the reflections of Rh metal and oxide are marked with blue and red lines, respectively.

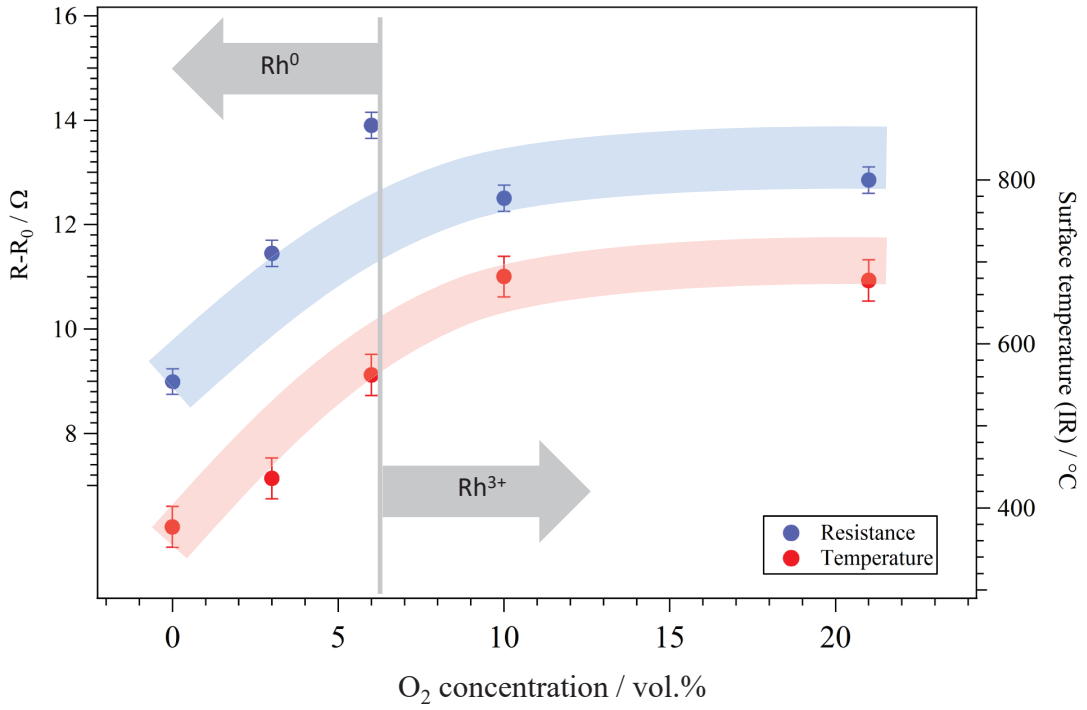


Figure 11: Influence of the chemical state of the Rh species on the electrical response and the surface temperature of the ceramic bead during the operation in 3.0 vol.% $CH_4$ atmosphere with different oxygen concentrations. The applied current is 100 mA for all the operation conditions.

Table 1: Pre-treatment conditions of the investigated samples.

| Sensor | Pre-treatment |
|---|---|
| fresh | approx. 12 h of operation (exposure to air) at 100 mA |
| conditioned | fresh sensor samples, additionally treated with approx. 4 h exposure to 50% LEL (EU) of 2.2 vol.% $CH_4$, 0.85 vol.% $C_3H_8$ and 2.0 vol.% $H_2$ in air |
| HMDS poisoned | conditioned and treated with 10 ppm hexamethyldisiloxane (HMDS) for 8 h, about 10% residual $CH_4$-sensitivity |
| $H_2S$ poisoned | conditioned and treated with 100 ppm $H_2S$ for 25 h, about 50% residual $CH_4$-sensitivity |

## Supporting Information Available

The following files are available free of charge:

Working principle and a built-up of a thermoresistive gas sensor; IR-thermograms of two fresh pellistors at 100 mA operation current in air; Results of the linear combination analysis (LCA) of Rh K XANES spectra; Results of the EXAFS analysis at Rh K-edge of fresh, conditioned and HMDS poisoned pellistors.

# References


(1) Safety-related parameter of the Physikalisch-Technische Bundesanstalt (PTB), valid in Europe. The value valid in USA is 5.0 vol.%.

(2) Kamieniak, J.; Randviir, E. P.; Banks, C. E. The latest developments in the analytical sensing of methane. *Trends in Analytical Chemistry* **2015**, *73*, 146–157.

(3) Moseley, P. T. Solid state gas sensors. *Measurement Science and Technology* **1997**, *8*, 223–237.

(4) Jessel, W., Ed. *Gase - Dämpfe - Gasmesstechnik: ein Kompendium für die Praxis*; Dräger Safety AG & Company KGaA, 2001.

(5) *International Electrotechnical Commission (IEC) 60079-29-1:2016-07 (en)*; VDE Verlag GmbH, 2016.

(6) Dabill, D. W.; Gentry, S. J.; Walsh, P. T. A fast-response catalytic sensor for flammable gases. *Sensors and Actuators* **1987**, *11*, 135–143.

(7) Oleksenko, L. P.; Fedorenko, G. V.; Maksymovych, N. P. Highly sensetive to methane sensor materails based on nano-Pd/SnO2. *Theoretical and Experimental Chemistry* **2019**, *55*, 132–136.

(8) Wang, H. C.; Hou, L. Y.; Zhang, W. Y. A drop-on-demand droplet generator for coatig catalytic materials on microhotplates of micropellistor. *Sensors and Actuators B-Chemical* **2013**, *183*, 342–349.

(9) Miller, J. B. Catalytic Sensors for Monitoring Explosive Atmospheres. *IEEE Sensors Journal* **2001**, *1*, 88.

(10) Palmer, T. H. Gas detecting apparatus. UK Patent 1023561, 1966.

(11) Dabill, D. W.; Gentry, S. J.; Hurst, N. W.; Jones, A.; Walsh, P. T. Catalytic gas-sensitive elements. UK Patent GB 2083630 B, 1984.

(12) *DrägerSensor & Portable Instruments Handbook*; Dräger Safety AG & Company KGaA, 2009.

(13) Chou, J., Ed. *Hazardous gas monitors: a practical guide to selection, operation and applications*; New York: McGraw-Hill, 2000.

(14) Kovar, USPTO United States Patent and Trademark Office "Trademark Assignment Abstract", 1993.

(15) Enger, B. C.; Lodeng, R.; Holmen, A. A review of catalytic partial oxidation of methane to synthesis gas with emphasis on reaction mechanisms over transition metal catalysts. *Applied Catalysis A-General* **2008**, *346*, 1–27.

(16) Lee, J. H.; Trimm, D. L. Catalytic combustion of methane. *Fuel Processing Technology* **1995**, *42*, 339–359.

(17) Li, L.; Niu, S. F.; Qu, Y.; Zhang, Q.; Li, H.; Li, Y. S.; Zhao, W. R.; Shi, J. L. One-pot synthesis of uniform mesoporous rhodium oxide/alumina hybrid as high sensitivity and low power consumption methane catalytic combustion micro-sensor. *Journal of Materials Chemistry* **2012**, *22*, 9263–9267.

(18) Hurtado, P.; Ordonez, S.; Vega, A.; Diez, F. V. Catalytic combustion of methane over commercial catalysts in presence of ammonia and hydrogen sulphide. *Chemosphere* **2004**, *55*, 681–689.

(19) Ryu, C. K.; Ryoo, M. W.; Ryu, I. S.; Kang, S. K. Catalytic combustion of methane over supported bimetallic Pd catalysts: Effects of Ru or Rh addition. *Catalysis Today* **1999**, *47*, 141–147.

(20) Müller, S. A.; Degler, D.; Feldmann, C.; Turk, M.; Moos, R.; Fink, K.; Studt, F.; Gerthsen, D.; Barsan, N.; Grunwaldt, J.-D. Exploiting synergies in catalysis and gas sensing using noble metal-loaded oxide composites. *ChemCatChem Concepts* **2018**, *10*, 864–880.

(21) Gelin, P.; Primet, M. Complete oxidation of methane at low temperature over noble metal based catalysts: a review. *Applied Catalysis B-Environmental* **2002**, *39*, 1–37.

(22) Shimizu, K.; Oda, T.; Sakamoto, Y.; Kamiya, Y.; Yoshida, H.; Satsuma, A. Quantitative determination of average rhodium oxidation state by a simple XANES analysis. *Applied Catalysis B-Environmental* **2012**, *111-112*, 509–514.

(23) Grunwaldt, J.-D.; Baiker, A. Axial variation of the oxidation state of Pt-Rh/Al2O3 during partial methane oxidation in a fixed-bed reactor: An in situ X-ray absorption spectroscopy study. *Catalysis Letters* **2005**, *99*, 5–12.

(24) Grunwaldt, J.-D.; Basini, L.; Clausen, B. S. In situ EXAFS study of Rh/Al2O3 catalysts for catalytic partial oxidation of methane. *Journal of Catalysis* **2001**, *200*, 321–329.

(25) Erdohelyi, A.; Cserenyi, J.; Solymosi, F. Activation of CH4 and Its Reaction with CO2 over Supported Rh Catalysts. *Journal of Catalysis* **1993**, *141*, 287–299.

(26) Monai, M.; Montini, T.; Gorte, R. J.; Fornasiero, P. Catalytic oxidation of methane: Pd and below. *European Journal of Inorganic Chemistry* **2018**, *25*, 2884–2893.

(27) Pakhare, D.; Spivey, J. A review of dry CO2 reforming of methane over noble metal catalysts. *Chemical Society Reviews* **2014**, *43*, 7813–7837.

(28) Stotz, H.; Maier, L.; Boubnov, A.; Gremminger, A. T.; Grunwaldt, J.-D.; Deutschmann, O. Surface reaction kinetics of methane oxidation over PdO. *Journal of Catalysis* **2019**, *370*, 152–175.

(29) Oudar, J. Sulfur adsorption and poisoning of metallic catalysts. *Catalysis Reviews-Science and Engineering* **1980**, *22*, 171–195.

(30) Ortloff, F.; Bohnau, J.; Kramar, U.; Graf, F.; Kolb, T. Studies on the influence of H2S and SO2 on the activity of a PdO/Al2O3 catalysts for removal of oxygen by total oxidation of (bio-) methane at very low O2:CH4 ratios. *Applied Catalysis B-Environmental* **2016**, *182*, 550–561.

(31) Gremminger, A.; Lott, P.; Merts, M.; Casapu, M.; Grunwaldt, J.-D.; Deutschmann, O. Sulfur poisoning and regeneration of bimetallic Pd-Pt methane oxidation catalysts. *Applied Catalysis B-Environmental* **2017**, *218*, 833–843.

(32) Lott, P.; Eck, M.; Doronkin, D. E.; Popescu, R.; Casapu, M.; Grunwaldt, J.-D.; Deutschmann, O. Regeneration of Sulfur Poisoned Pd-Pt/CeO2-ZrO2-Y2O3-La2O3 and Pd-Pt/Al2O3 Methane Oxidation Catalysts. *Topics in Catalysis* **2019**, *62*, 164–171.

(33) Zhang, Y.; Glarborg, P.; Johansen, K.; Andersson, M. P.; Torp, T. K.; Jensen, A. D.; Christensen, J. M. A Rhodium-Based Methane Oxidation Catalyst with High Tolerance to H2O and SO2. *ACS Catalysis* **2020**, *10*, 1821–1827.

(34) Meeyoo, V.; Trimm, D. L.; Cant, N. W. The effect of sulphur containing pollutants on the oxidation activityof precious metals used in vehicle exhaust catalysts. *Applied Catalysis B-Environmental* **1998**, *16*, L101–L104.

(35) Nasri, N. S.; Jones, J. M.; Dupont, V. A.; Williams, A. A comparative study of sulfur poisoning and regeneration of precious-metal catalysts. *Energy Fuels* **1998**, *12*, 1130–1134.

(36) Xie, C. Understanding of catalyst deactivation caused by sulfur poisoning and carbon deposition in strea reforming of liqiud hydrocarbon fuels. Ph.D. thesis, The Pennsylvania State University, 2011.

(37) Ajhar, M.; Travesset, M.; Yuce, S.; Melin, T. Siloxane removal from landfill and degester gas - A technology overview. *Bioresource Technology* **2010**, *101*, 2913–2923.

(38) Finocchio, E.; Montanari, T.; Garuti, G.; Pistarino, C.; Federici, F.; Cugino, M.; Busca, G. Purification of biogases from siloxane by adsorption: on the regenerability of activated carbon sorbents. *Energy Fuels* **2009**, *23*, 4156–4159.

(39) Haga, K.; Adachi, S.; Shiratori, Y.; Itoh, K.; Sasaki, K. Poisoning of SOFC anodes by various fuel impurities. *Solid State Ionics* **2008**, *179*, 1427–1431.

(40) Urban, W.; Lohmann, H.; Gomez, J. I. S. Catalysically upgraded landfill gas as a cost-effective alternative for fuel cells. *Journal of Power Sources* **2009**, *193*, 359–366.

(41) Hannemann, S.; Grunwaldt, J.-D.; van Vegten, N.; Baiker, A.; Boye, P.; Schroer, C. G. Distict spatial changes of the catalyst structure inside a fixed-bed microreactor during the partial oxidation of methane over Rh/Al2O3. *Catalysis Today* **2007**, *126*, 54–63.

(42) Chen, Y. S.; Xie, C.; Li, Y.; Song, C. S.; Bolin, T. B. Sulfur poisoning mechanism of steam reforming catalysts: an X-rayabsorption near edge structure (XANES) spectroscopic study. *Physical Chemistry Chemical Physics* **2010**, *12*, 5707–5711.

(43) Spangenberg, T.; Göttlicher, J.; Steininger, R. An Efficient Referencing And Sample Positioning System To Investigate Heterogeneous Substances With Combined Microfocused Synchrotron X-ray Techniques. *AIP Conference Proceedings* **2009**, *1092*, 93.

(44) Zimina, A.; Dardenne, K.; Denecke, M. A.; Doronkin, D. E.; Huttel, E.; Lichtenberg, H.; Mangold, S.; Pruessmann, T.; Rothe, J.; Spangenberg, T.; Steininger, R.; Vitova, T.; Geckeis, H.; Grunwaldt, J.-D. CAT-ACT—A new highly versatile x-ray spectroscopy beamline for catalysis and radionuclide science at the KIT synchrotron light facility ANKA. *Review of Scientific Instruments* **2017**, *88*, 113113.

(45) Ravel, B.; Newville, M. ATHENA, ARTEMIS, HEPHAESTUS: data analysis for X-ray absorption spectroscopy using IFEFFIT. *Journal of Synchrotron Radiation* **2005**, *12*, 537–541.

(46) Kozlov, A. G. Optimization of structure and power supply conditions of catalytic gas sensor. *Sensors and Actuators B-Chemical* **2002**, *82*, 24–33.

(47) Jalilehvand, F. Sulfur: not a "silent" element any more. *Chemical Society Reviews* **2006**, *35*, 1256–1268.

# Graphical TOC Entry